Front. Energy 2017, 11(1): 4–22
DOI 10.1007/s11708-016-0442-6

RESEARCH ARTICLE

Nitin NAMPALLI, Tsun Hang FUNG, Stuart WENHAM, Brett HALLAM, Malcolm ABBOTT

Statistical analysis of recombination properties of the boron-oxygen defect in p-type Czochralski silicon

Abstract This paper presents the application of lifetime spectroscopy to the study of carrier-induced degradation ascribed to the boron-oxygen (BO) defect. Specifically, a large data set of p-type silicon samples is used to investigate two important aspects of carrier lifetime analysis: ① the methods used to extract the recombination lifetime associated with the defect and ② the underlying assumption that carrier injection does not affect lifetime components unrelated to the defect. The results demonstrate that the capture cross section ratio associated with the donor level of the BO defect (k_1) vary widely depending on the specific method used to extract the defect-specific recombination lifetime. For the data set studied here, it was also found that illumination used to form the defect caused minor, but statistically significant changes in the surface passivation used. This violation of the fundamental assumption could be accounted for by applying appropriate curve fitting methods, resulting in an improved estimate of k_1 (11.90±0.45) for the fully formed BO defect when modeled using the donor level alone. Illumination also appeared to cause a minor, apparently injection-independent change in lifetime that could not be attributed to the donor level of the BO defect alone and is likely related to the acceptor level of the BO defect. While specific to the BO defect, this study has implications for the use of lifetime spectroscopy to study other carrier induced defects. Finally, we demonstrate the use of a unit-less regression goodness-of-fit metric for lifetime data that is easy to interpret and accounts for repeatability error.

Keywords Czochralski silicon, boron-oxygen defect, injection dependent lifetime spectroscopy, goodness-of-fit, repeatability error

Received July 22, 2016; accepted October 19, 2016

Nitin NAMPALLI (✉), Tsun Hang FUNG, Stuart WENHAM, Brett HALLAM, Malcolm ABBOTT
School of Photovoltaic and Renewable Energy Engineering, University of New South Wales, Sydney, NSW 2052, Australia
E-mail: n.nampalli@unsw.edu.au

1 Introduction

The boron-oxygen (BO) defect is an important lifetime-limiting defect in p-type silicon, potentially reducing the efficiency of commercial cells by 1%–2% absolute [1]. Despite its importance however, there exist only a limited number of studies on the recombination characteristics of BO defects, none which employ large, statistically robust data sets. This study explores some important issues relating to the BO defect's recombination properties and their implications for carrier lifetime analysis.

The recombination behavior of BO defects has been typically described by Shockley-Read-Hall (SRH) trap-assisted recombination [2], and has been studied using a range of different methods, namely deep level transient spectroscopy (DLTS) [3], injection-dependent lifetime spectroscopy (IDLS) [4–14] and temperature-dependent lifetime spectroscopy (TDLS) [6,15]. There is broad agreement in the literature about some aspects of the defect; however, the various studies differ somewhat in their conclusions regarding the SRH recombination characteristics of the defect.

What is known with confidence is that there are two distinct defect levels associated with the fully formed BO defect — a deep donor level ($E_{trap,1}$) situated 0.41 eV below the conduction band (E_C) [3–6] and an acceptor level ($E_{trap,2}$) situated above the valence band energy level (E_V) [3,8,9]. The deep donor level acts as a minority carrier trap in p-type silicon and is largely responsible for lifetime degradation in p-type silicon as it dominates at low to medium injection conditions. The acceptor level, on the other hand, is a majority carrier trap in p-type silicon and has a smaller impact on carrier lifetime in p-type silicon and then too, is thought to affect lifetime only at high injection [4,6]. In fact, a number of studies on the fully formed BO defect in p-type silicon have reported good fits to IDLS data using a single defect model with a single trap level (i.e. using $E_{trap,1}$ alone) [6,10,13]. In contrast to p-type silicon, carrier lifetime in compensated n-type material appears to be strongly affected by both the

donor level (majority carrier trap in n-type silicon) and the acceptor level (minority carrier trap in n-type silicon) [5,8,9,11,12], and therefore requires a two-level defect model (i.e. using $E_{trap,1}$ and $E_{trap,2}$) to adequately describe the injection dependence of carrier lifetime.

The second well known property of the BO defect is that the CID effect occurs in two stages—a fast degradation stage and a slow degradation stage. This has been well-characterized in p-type silicon [7,14] but is also suspected to occur in compensated n-type silicon [9,12], albeit at a much slower rate than in p-type silicon. Further, the characteristic injection-dependence of carrier lifetime associated with the fast stage appears to require a significantly higher capture cross section ratio to adequately fit the measured data compared to the slow stage [7,9,12]. This has important implications for the study of the fully formed defect (i.e. after complete degradation) in compensated n-type material, in which the fast stage is more dominant and therefore requires a correction factor [9] to be applied when studying the slow stage in such material [12]. In contrast, lifetime in p-type silicon after complete degradation is known to be largely dominated by the slow degradation stage [7]. Considering also that $E_{trap,1}$ appears to be more dominant in p-type material, as previously noted, characterization of the fully formed defect in p-type material using a single defect model with a single trap level has therefore provided important insights into the property of the $E_{trap,1}$ level and is the primary focus of this work.

However, even when a single defect level in p-type silicon has been used to describe the fully formed BO defect, there have been three major inconsistencies in the literature regarding the determination of recombination properties of the BO defect based on IDLS data. First, the electron-to-hole carrier capture cross section ratio associated with $E_{trap,1}$ ($k_1 = \sigma_{n1}/\sigma_{p1}$) was proposed to be in the range of 9–10 based on IDLS and TDLS data assuming a single defect model with a single trap level [4–6]; however, a small number of studies have determined k_1 values in p-type silicon to be higher—between 10 and 12 [8]. A similar value was obtained in another study on samples with the BO defects deactivated [13], although values as high as 16–23 have also been reported for the fully active BO defect [14]. The reason why such a broad range in observed k_1 values exists is currently unknown. Given that the few studies on the fully formed defect in which the p-type base doping levels were varied (1–30 Ω·cm in Ref. [4], 0.5–3.5 Ω·cm in Ref. [6]) do not explicitly report variations in k_1 with base doping—and indeed report a single k_1 value—it appears likely that the variation in reported k_1 is due to other unknown reasons. Attempts to explore this have also been limited by a lack of knowledge about the expected statistical variability in k_1 for a sample set of similar wafers.

Secondly, the primary assumption made in most studies is that processes used to manipulate the state of the BO defect only affects the SRH lifetime associated with the BO defect, $\tau_{SRH,BO}$. Since any changes in non-BO related lifetime components such as the surface/emitter lifetime (τ_{surf}) and non-BO related bulk lifetime could potentially affect the estimation of $\tau_{SRH,BO}$ and therefore the value of k_1, it is important that any such changes are accounted for. Although minor, evidence of such changes are visible in IDLS data presented in some early studies [4–6]; however, there have been no explicit attempts to quantify such changes. The magnitude of such changes, and their impact on the determination of k_1 therefore remains unknown.

Thirdly, methods used to determine k_1 from IDLS data vary slightly between studies. In most studies, the inverse lifetime after complete deactivation of the BO defect via dark annealing (τ_{DA}^{-1}) is subtracted from the inverse lifetime after complete activation of the defect after light soaking (τ_{LS}^{-1}), with the difference ($\tau_{LS}^{-1}-\tau_{DA}^{-1}$) then fitted to determine k_1 [4–6,8,11]. However, in other studies, k_1 is determined by attempting to fit τ_{LS} rather than ($\tau_{LS}^{-1}-\tau_{DA}^{-1}$) based on certain assumptions about τ_{DA} [10,13,14]. The impact of the various fitting methods, the assumptions made about τ_{DA} and the ability of these methods to account for change in non-BO related lifetime on the fitted values of k_1 has not been quantified, making it difficult to determine which method is more accurate.

In this work, we present statistical analysis of IDLS data from a large data set of commercial p-type wafers to address these unanswered questions. In particular, multiple methods for analyzing IDLS data from BO-afflicted samples are evaluated to validate the underlying assumption regarding changes in non-BO related lifetime under exposure to illumination. We discuss the implications of these assumptions on IDLS and TDLS characterization and present revised values of k_1 for the BO defect assuming a single defect model with a single trap level.

2 Experimental method

In this study, commercial grade 156 mm × 156 mm pseudo-square boron-doped Cz wafers (1.6 Ω·cm) were used to create symmetric lifetime test structures. A saw damage etch was performed on the as-received wafers, followed by alkaline texturing and acidic neutralisation. Wafers were then subjected to an RCA clean and HF dip, then diffused at 795°C for 25 min in a $POCl_3$ tube furnace followed by a drive-in diffusion at 885°C for 30 min to achieve an emitter sheet resistance of 70 Ω/sq—a process known to be effective at gettering [16].

The phosphosilicate glass (PSG) and emitter thus formed were removed by etching ~2 μm from both surfaces, resulting in a wafer thickness of approximately 180 μm. This was done to ensure minimal concentrations of impurities other than BO within the wafer bulk. The wafers were then RCA cleaned and followed by a second, light $POCl_3$ diffusion at 780°C for 30 min with a 20 min

drive-in step to achieve a sheet resistance of ~200 Ω/sq. This was done to aid in surface passivation and minimize the influence of changes in surface recombination on carrier lifetime during further processing. The PSG resulting from this second diffusion was etched off in dilute HF, followed by the deposition of SiN_x:H dielectric layers on both sides of the wafers using a Roth & Rau MAiA plasma-enhanced chemical vapor deposition (PECVD) system. All SiN_x:H layers deposited were 80 nm thick and had a refractive index of 2.08 at 633 nm.

A total of 25 wafers were so processed. All samples were then dark annealed at 200°C for 15 min (to ensure complete temporary deactivation of the BO defect) followed by a light soak under halogen lights at an intensity equivalent to 0.78 suns at 35°C for 48 h to ensure complete activation of the BO defect. The effective carrier lifetime was measured on nine sampling points for all wafers after complete deactivation and after complete activation of the BO defect using the WCT-120 (Sinton Instruments) photoconductance decay (PCD) lifetime tester [17]. Ambient light exposure prior to measurement was minimized by maintaining all samples in the dark between the dark anneal step and the subsequent lifetime measurement. Further, the measurement tool was maintained in a darkened chamber during measurement to minimize any unintentional biasing of the sample during measurement. A flash lamp with an added infrared filter was used as the variable light source for measurements. The measured IDLS data was analyzed using the generalized method [18] and corrected for intrinsic recombination (i.e. Auger and radiative recombination) using the Richter model [19]. The resulting injection dependent data obtained after accounting for intrinsic recombination is hereby referred to as τ_{DA} (measured after dark annealing) and τ_{LS} (measured after light soaking). Unless otherwise specified, all lifetime values reported in this work refer to measured values at an injection level corresponding to $\Delta n = 0.1 \times N_A$ after accounting for intrinsic recombination.

3 Analytical approach

A description of the lifetime components used, the approach used to determine each component and the metrics relevant to describing the BO defect properties are discussed in this section.

3.1 Carrier lifetime model

The inverse lifetime of a sample containing BO defects can be modeled as the sum of a series of inverse lifetime components to account for recombination related to BO defects as well as from other sources of recombination. In this study, τ_{DA} was assumed to be described by three lifetime components representing recombination in the surface region (τ_{surf}), an injection independent bulk recombination component ($\tau_{bulk,non\text{-}BO}$) and an injection dependent SRH recombination component ($\tau_{SRH,non\text{-}BO}$). τ_{LS} was then assumed to contain an additional lifetime component representing SRH recombination due to the BO defect ($\tau_{SRH,BO}$). Having already accounted for intrinsic recombination, as noted earlier, τ_{DA}^{-1} and τ_{LS}^{-1} were thus modeled as follows:

$$\frac{1}{\tau_{DA}} = \frac{1}{\tau_{surf}} + \frac{1}{\tau_{bulk,fixed}} + \frac{1}{\tau_{SRH,non\text{-}BO}}, \quad (1)$$

$$\frac{1}{\tau_{LS}} = \frac{1}{\tau_{surf}} + \frac{1}{\tau_{bulk,fixed}} + \frac{1}{\tau_{SRH,non\text{-}BO}} + \frac{1}{\tau_{SRH,BO}}. \quad (2)$$

Note that the lifetime components specified in Eq. (1) were chosen in order to achieve acceptable fits to τ_{DA} across a broad range of injection levels. This is explained further below and in Section 4. For now, we discuss details about the individual lifetime components. τ_{surf} is assumed to be dependent on the emitter saturation current (J_{0e}) through the following relation which applies for samples with symmetric surfaces/emitters [20]:

$$\frac{1}{\tau_{surf}} = 2J_{0e} \times \frac{(N_A + \Delta n)}{qWn_i^2}. \quad (3)$$

N_A, Δn, n_i^2, W and q in Eq. (3) refer to the bulk doping concentration, excess minority carrier concentration, intrinsic carrier concentration, sample thickness and fundamental charge constant respectively. N_A for the samples in this study was determined to be 9.14×10^{15} cm^{-3} via 4-point probe measurements performed prior to the emitter diffusion. All carrier concentrations in the model (n, p, and n_i^2) were calculated at steady-state as a function of Δn using Fermi-Dirac statistics taking into account band-gap narrowing [21,22] and potential degeneracy effects [23]. The SRH recombination terms ($\tau_{SRH,BO}$ and $\tau_{SRH,non\text{-}BO}$) are assumed to be described by a single defect with a single trap level as follows:

$$\frac{1}{\tau_{SRH}} = \frac{(np - n_i^2)}{\Delta n[\tau_{n0}(n + n_1) + \tau_{p0}(p + p_1)]}. \quad (4)$$

Here, n and p are the total electron and hole concentrations, τ_{n0} and τ_{p0} are the SRH-related electron and hole recombination lifetimes, and n_1 and p_1 represent the SRH-related electron and hole populations characteristic of the trap level within the bandgap. τ_{n0} and τ_{p0} are further related to the defect capture cross section ratio, k, through the following relation:

$$k = \frac{\sigma_n}{\sigma_p} = \frac{\tau_{p0}}{\tau_{n0}} \times \frac{v_h}{v_e}. \quad (5)$$

Here, v_e and v_h are the electron and hole thermal velocities respectively [24]. Note that a number of studies in the literature have ignored the contribution to k of (v_e/v_h), which has a value of 1.208 at 300 K. This has resulted

in an overestimation of k in such studies [5,10,13]. For the sake of consistency, the impact of (v_e/v_h) has been taken into account where values of k are quoted from literature.

$\tau_{SRH,non\text{-}BO}$ was found to be best described by a mid-gap trap level with a fixed k value of 100. Although this is similar to the value expected for interstitial iron, samples were confirmed to have negligible concentrations of iron [25] and it was ruled out that $\tau_{SRH,non\text{-}BO}$ represents any carrier-induced defects. Therefore, $\tau_{SRH,non\text{-}BO}$ represents other bulk defects that are not light-activated. Together with $\tau_{bulk,fixed}$, $\tau_{SRH,non\text{-}BO}$ so defined was found to adequately describe any injection-dependence in bulk lifetime in τ_{DA}, thus allowing injection dependent effects in τ_{LS} specific to the BO defect to be fully described by $\tau_{SRH,BO}$.

$\tau_{SRH,BO}$ was also assumed to be described by a single trap level, $E_{trap,1}$ at $E_C - 0.41$ eV [3,6], with the capture cross section ratio, k_1, allowed to vary during fitting. Note that the contribution of the acceptor level of the BO defect ($E_{trap,2}$) has not been included in $\tau_{SRH,BO}$. As will be discussed later, this approach was justified for the p-type samples used in this work. Nevertheless, any potential changes in lifetime related to $E_{trap,2}$ that display strong injection-dependence in high injection [4,6] or are approximately injection-independent in p-type silicon [11,14] are expected to be accounted for by changes in τ_{surf} and $\tau_{bulk,fixed}$ respectively. Separate from this, any injection-dependent changes in the bulk unrelated to the BO defect are expected to be accounted for by changes in $\tau_{SRH,non\text{-}BO}$. A detailed discussion about the influence of $E_{trap,2}$ is presented later in Sections 5.3 and 5.5.

3.2 IDLS modeling approach

Considered together, τ_{DA} and τ_{LS} can be thought of as containing information about the four components of the lifetime model noted in Eqs. (1) and (2). The parameters describing these components can be deduced in a number of ways depending on which IDLS curve is used to extract the parameters and how the parameters are constrained during regression fitting. While τ_{surf}, $\tau_{bulk,fixed}$, and $\tau_{SRH,non\text{-}BO}$ can be extracted from τ_{DA}, from τ_{LS} or from a combination of τ_{LS} and τ_{DA}, $\tau_{SRH,BO}$ can only be extracted from τ_{LS} or from the difference in inverse lifetime ($\tau_{LS}^{-1} - \tau_{DA}^{-1}$). Further, in the case where all lifetime components from τ_{DA} are assumed to apply to τ_{LS}, the constraints on possible values of the fitting parameters can be different depending on whether τ_{DA} and τ_{LS} are fitted separately or simultaneously. Thus, a number of fitting methods may be used, with the overall goal being to determine methods of extracting the lifetime components that not only result in the best fit to the experimental data but are also physically meaningful.

To guide the choices of methods, we attempted to test two hypotheses in this study. First, we test the hypothesis that light soaking causes only $\tau_{SRH,BO}$ to change between τ_{DA} and τ_{LS}. To do this, the measured IDLS data was modeled in 2 ways: by constraining all of the three components comprising τ_{DA} during τ_{LS} fitting (referred to as constrained methods), or by constraining some but not all of the three components (partially unconstrained). Comparing results from the constrained and partially unconstrained methods is therefore expected to reveal not only the presence of changes in lifetime between τ_{LS} and τ_{DA} not attributable to $\tau_{SRH,BO}$, but also which of the three remaining lifetime components best describes the changes.

Three types of constrained methods were used in this study. The first of these is the subtraction method (method A), in which τ_{DA}^{-1} was subtracted from τ_{LS}^{-1} and the resulting curve was modeled using $\tau_{SRH,BO}$ alone. τ_{DA} was then separately modeled to determine the other three lifetime components (τ_{surf}, $\tau_{bulk,fixed}$, and $\tau_{SRH,non\text{-}BO}$), leaving τ_{LS} to be described by the sum of the contributions of all four components. Note that explicit fits to τ_{LS} were not attempted in this method. The second constrained method was the 'separate' method (method B) in which τ_{DA} was first fitted to determine the parameters describing τ_{surf}, $\tau_{bulk,fixed}$, and $\tau_{SRH,non\text{-}BO}$. These parameters were then fixed in the subsequent fitting of the τ_{LS} curve, which included the $\tau_{SRH,BO}$ component. Thus, $\tau_{SRH,BO}$ was determined from the fit to τ_{LS} in this method rather than the fit to ($\tau_{LS}^{-1} - \tau_{DA}^{-1}$) as in the subtraction method. Lastly, in the 'simultaneous' method (method C), parameters for all lifetime components are solved for simultaneously rather than separately. This is done by simultaneous regression fitting of τ_{LS} and τ_{DA}, where $\tau_{SRH,BO}$ was assumed to contribute only to τ_{LS}. Thus, in summary, information about τ_{surf}, $\tau_{bulk,fixed}$, and $\tau_{SRH,non\text{-}BO}$ is effectively determined from τ_{DA} in methods A and B and from a combination of τ_{LS} and τ_{DA} in method C, whereas information regarding $\tau_{SRH,BO}$ is determined from ($\tau_{LS}^{-1} - \tau_{DA}^{-1}$) in method A, and from τ_{LS} alone in methods B and C.

The partially unconstrained methods followed a similar procedure to the 'separate' method, where τ_{DA} was fit first to determine τ_{surf}, $\tau_{bulk,fixed}$, and $\tau_{SRH,non\text{-}BO}$. However, in contrast to the constrained methods, the fitting parameters were not all unconstrained during τ_{LS} fitting. In methods D, E and F, only τ_{surf}, $\tau_{bulk,fixed}$, and $\tau_{SRH,non\text{-}BO}$ respectively were unconstrained. Thus, method D corresponds to the case where only a change in surface lifetime was assumed to occur between τ_{DA} and τ_{LS} measurement (i.e. during light soaking or between measurements). Methods E and F, in contrast, correspond to cases where only the bulk-related lifetime components are assumed to change. Whereas method E allows for an injection-independent change in bulk lifetime via $\tau_{bulk,fixed}$, method F allows for changes in bulk lifetime that are injection-dependent in the low injection regime ($\Delta n \leqslant 0.01 \times N_A$) via $\tau_{SRH,non\text{-}BO}$. We also allowed for the possibility that changes in surface lifetime and injection-independent bulk lifetime occur simultaneously by allowing both τ_{surf} and

$\tau_{bulk,fixed}$ to be free (method G), as well as the possibility that surface lifetime and injection-dependent bulk lifetime in low injection occur simultaneously (method H) by allowing τ_{surf} and $\tau_{SRH,non\text{-}BO}$ to vary between τ_{DA} and τ_{LS} fitting.

The second hypothesis tested in this study is whether it is possible to determine $\tau_{SRH,non\text{-}BO}$ in the absence of τ_{DA} measurements, as was done in some previous studies [14]. To do this, we perform fitting only to τ_{LS} using all four lifetime components (method I). τ_{DA} is then assumed to be described by removing the contribution of $\tau_{SRH,non\text{-}BO}$. Lastly, to determine the impact of other SRH defects in the bulk on the determination of $\tau_{SRH,BO}$, we attempted to fit τ_{LS} without $\tau_{SRH,non\text{-}BO}$ in method J (i.e. using only three of the four components: τ_{surf}, $\tau_{bulk,fixed}$ and $\tau_{SRH,BO}$). Comparing fits to τ_{DA} and τ_{LS} from methods I and B is therefore expected to reveal if accurate parameters for all components can be determined from τ_{LS} alone, whereas comparing methods I and J is expected to reveal the impact of ignoring non-BO related SRH defects on the determination of k_1.

Note that in all partially and fully unconstrained methods, information regarding $\tau_{SRH,BO}$ was deduced from fits to τ_{LS} only (as in method B) rather than from simultaneous fitting of τ_{DA} and τ_{LS} (method C) or from $(\tau_{LS}^{-1} - \tau_{DA}^{-1})$ (as in method A).

A summary of the methods described above and the IDLS curves from which the different lifetime components are extracted are presented in Table 1. Where relevant, references to previous IDLS studies utilizing the methods are also noted.

3.3 Regression and statistical analysis

Fitting of IDLS curves was performed by minimizing the sum of the squared residual terms (SSQ) using a quasi-Newton nonlinear regression algorithm. In addition to the SSQ between the measured inverse lifetime data and model output (SSQ_{data}), an extra SSQ term related to the difference in slopes of the inverse lifetime for the injection range $10^{14} < \Delta n < 10^{16}$ cm^{-3} (SSQ_{slope}) was calculated and given a 10% weight. The sum of the weighted terms was then minimized. The use of both terms was found to result in faster and more reliable convergence as the regression algorithm tended to converge at local minima in the parameter space when SSQ_{slope} was not weighted.

3.3.1 Goodness-of-fit metric

The goodness-of-fit (GOF) between the IDLS data and the model output was determined using a reduced Chi-square metric (Q), which is calculated as follows:

$$Q = \frac{\sum_{i=1}^{N} [(x_i - \mu_i)/\sigma_i]^2}{\mathrm{DOF}}. \quad (6)$$

In the above equations, x_i and μ_i refer to the inverse lifetime from the model and measured data respectively after correction for intrinsic recombination. σ_i refers to the variance in μ_i. DOF is the degrees of freedom remaining after model fitting and is calculated as the difference between the total number of fitted data points (N) and the number of variable fitting parameters used in the model (r).

Since the overall accuracy of a model being tested depends on the GOF associated with both τ_{LS} and τ_{DA}, it is useful to define a global GOF for the model (Q_{global}) in addition to the Q value associated with τ_{LS} (Q_{LS}). Q_{global} is calculated similarly to Eq. (7) by including x_i and μ_i terms from both τ_{LS} and τ_{DA}, and adding the corresponding N and r terms for DOF calculation. Note that fit parameters to describe τ_{DA} are obtained from the τ_{LS} model fits for methods I and J to reflect the source of the fitted components. In contrast, for the partially unconstrained methods (methods D–H), parameters for τ_{DA} are sourced from method B to reflect the assumption underlying these methods that light soaking causes changes in fit para-

Table 1 Summary of fitting methods

Type	ID	Description	IDLS curve used to extract lifetime components				References
			τ_{surf}	$\tau_{bulk,fixed}$	$\tau_{SRH,non\text{-}BO}$	$\tau_{SRH,BO}$	
Constrained	A	Subtraction	τ_{DA}	τ_{DA}	τ_{DA}	$(\tau_{LS}^{-1} - \tau_{DA}^{-1})$	[4–6,11]
	B	Separate	τ_{DA}	τ_{DA}	τ_{DA}	τ_{LS}	[10,14]
	C	Simultaneous	τ_{DA}, τ_{LS}	τ_{DA}, τ_{LS}	τ_{DA}, τ_{LS}	τ_{LS}	—
Partially unconstrained	D	Free τ_{surf}	τ_{LS}	τ_{DA}	τ_{DA}	τ_{LS}	—
	E	Free $\tau_{bulk.fixed}$	τ_{DA}	τ_{LS}	τ_{DA}	τ_{LS}	—
	F	Free $\tau_{SRH,non\text{-}BO}$	τ_{DA}	τ_{DA}	τ_{LS}	τ_{LS}	—
	G	Free τ_{surf}, $\tau_{bulk,fixed}$	τ_{LS}	τ_{LS}	τ_{DA}	τ_{LS}	—
	H	Free τ_{surf}, $\tau_{SRH,non\text{-}BO}$	τ_{DA}	τ_{LS}	τ_{LS}	τ_{LS}	—
Free / fully unconstrained	I	All free	τ_{LS}	τ_{LS}	τ_{LS}	τ_{LS}	—
	J	All free (no $\tau_{SRH,non\text{-}BO}$)	τ_{LS}	τ_{LS}	—	τ_{LS}	[14]

meters, as described in Section 3.2. Finally, the constrained methods (methods A, B and C) use the τ_{DA} parameters determined from the respective methods.

The reduced Chi-square metric defined above is essentially a unit-less ratio of the residual error associated with the model relative to the expected point-to-point variability in the data. Hence, a Q value of 1 signifies a good fit to the data within the expected measurement uncertainty; whereas Q values significantly greater than 1 indicate poor fits wherein the residual error is greater than what might be expected due to variance in the data. Q values may also be less than 1, with values significantly lower than 1 suggesting that the model is 'over-fitting' the data. This can occur when r is a large fraction of N, or when σ_i is overestimated. This simplicity of interpretation is a significant advantage of Q over GOF metrics used in other IDLS studies such as mean squared error [26] and non-normalized Chi-square [6], which are not unit-less and do not account for repeatability error. This makes them impractical for comparing GOF measures between studies. Also, while GOF metrics for nonlinear models that are more robust than Q do exist, they are computationally intensive [27] and were therefore not considered for this analysis.

However, the ability to draw meaningful conclusions from Q depends on accurate estimation of DOF and σ_i. We note that DOF calculated as above is likely an underestimation as IDLS curves are nonlinear with respect to Δn and, strictly speaking, DOF can vary between 0 to $(N - r)$ depending on the degree of nonlinearity of the model [27]. Further, since the inclusion of $\tau_{SRH,BO}$ causes significant changes in the degree of nonlinearity of the IDLS curves, and increases r between τ_{DA} fitting ($r \leqslant 4$) and τ_{LS} fitting ($r \leqslant 5$), the Q_{LS} for a particular sample analyzed using one method may not be directly comparable to Q_{DA} or Q_{global} from another sample fit using a different method. However, considering that the maximum number of free parameters ($r \leqslant 5$) is at least an order of magnitude less than the number of data points within an IDLS curve ($80 < N < 179$ for all samples), Q values for a given sample are still comparable. Further, the large number of IDLS curves (225) allows aggregate behavior across samples to be compared, making Q an acceptable metric for comparative analysis of fitting methods.

We now consider the implications of σ_i. There are three contributors to total error for any measurement depending on the source of the error: repeatability error, reproducibility error, and measurement artifacts. While repeatability error quantifies differences in measured values with time using the same instrument, reproducibility error quantifies differences in measured value between instruments [28,29]. In contrast, measurement artifacts are deviations from the true value that stem from the specific measurement method or technique. Note that for practical purposes, repeatability and/or reproducibility error may be quantified and used as is in Eq. (6), whereas measurement artifacts either need to be corrected, prevented or removed by screening the measured data.

The approach used in this study to quantify σ_i was to (a) minimize the tool-specific sources of error where feasible such that the difference between the reproducibility and repeatability errors are minimal, (b) minimize the impact of artifacts, and (c) quantify the remaining error via measurements of the repeatability error. Tool-specific errors were minimized via careful and regular calibration of the tool between measurements. While the component of reproducibility error specific to the tool could not be feasibly quantified and may be nonzero, we make the assumption here that reproducibility and repeatability error are now equal. We now discuss the issue of minimizing measurement artifacts.

Carrier lifetime measurements using the PCD technique are known to introduce measurement artifacts– particularly in low injection — due to trapping effects [30] and depletion region modulation (DRM) [31]. Further, any ambient light present during measurement could lead to unintentional biasing, leading to additional error in low injection conditions. Measurement error could also be introduced at high injection if the reference cell used to measure the illumination intensity of the flash lamp is saturated. Considering the cumbersome nature of quantifying the magnitude of error introduced by each of these effects and the large data set involved, it was decided to minimize and screen for artifacts, rather than apply corrections, which may themselves be a source of error. As noted in Section 2, the impact of unintentional bias at low injection from stray light was first minimized by performing all measurements in the dark. Secondly, only lifetime data within a specific range of Δn was used for regression. The upper limit of Δn varied between samples and was ensured to be below the injection level that caused saturation of the reference cell (roughly $\Delta n = 3.3 \times 10^{16}$ cm^{-3}), whereas the lower limit of acceptable Δn was set to a single value for all samples ($\Delta n = 6 \times 10^{13}$ cm$^{-3} \approx 0.006 \times N_A$), which was chosen to be greater than the onset injection level below which DRM and trapping effects were found to dominate lifetime for a wide range of samples. Using these methods, measurement artifacts were largely eliminated from the data set used for regression.

Since all measurements in this study were performed on similarly processed wafers on the same instrument, with lifetime extracted using the same method (generalized), σ_i can now be estimated by the repeatability error alone.

3.3.2 Estimation of uncertainty

The reproducibility error associated with PCD-based IDLS measurements analyzed using the generalized method is known to have a significant injection dependence and is estimated to be about 10% for $\Delta n = 10^{15}$ cm^{-3} [25]. Since attempting to set σ_i = 10% of x_i resulted in Q values significantly less than 1, it was concluded that the

repeatability error was lower than 10%. We therefore performed direct measurements of the repeatability error as a function of Δn. This was done by removing and replacing the same sample at approximately the same wafer position on the measurement area between 10 measurements. The standard deviation of the measured lifetime was then calculated at each injection level to obtain the repeatability error in inverse lifetime. This procedure was repeated for all 9 measurement points on the wafer, resulting in a total of 90 IDLS curves for σ_i estimation. The standard deviations were then averaged across all measurement points and fitted empirically. The resulting average σ_i as a function of Δn is plotted below in Fig. 1.

As Fig. 1 shows, σ_i was almost constant (about 0.80%) for $\Delta n > 3.45 \times 10^{14}$ cm^{-3} and increased almost linearly on a log-log scale for lower Δn. σ_i (Δn) could be modeled using an empirical function given in Eq. (7). Note that although σ_i is parameterized specifically for inverse lifetime (e.g. τ_{DA}^{-1}), the repeatability error in lifetime (e.g. τ_{DA}) is also approximately the same.

$$\sigma_i(\Delta n) = \begin{cases} 13.62\%, & \Delta n \leqslant 2 \times 10^{13}\ \text{cm}^{-3} \\ e^{[-0.9737 \times \ln(\Delta n) + \ln(1.14 \times 10^{12})]}, & 2 \times 10^{13} \leqslant \Delta n \leqslant 3.45 \times 10^{14}\ \text{cm}^{-3} \\ 1.413\%, & \Delta n \geqslant 3.45 \times 10^{14}\ \text{cm}^{-3} \end{cases}. \quad (7)$$

While the underlying causes of error are beyond the scope of this study, we note that the dependence of σ_i on Δn is comparable to that of the reproducibility error reported in Ref. [25] and suggests that the same uncertainties that lead to high reproducibility error may also be responsible for increased repeatability error in low injection conditions. Further, measurement points on the wafer closer or further from the edges may be differently affected by edge recombination and trapping effects [30]. Likewise, doping non-uniformity and thickness variations may cause depletion region modulation as well as trapping effects to be triggered at slightly different Δn [31]. Such variations can explain the increased σ_i in low injection.

Finally, we note that while the repeatability error measured above was performed for $\Delta n > 2 \times 10^{13}$ cm^{-3}, only data for $\Delta n > 6 \times 10^{13}$ cm^{-3} was actually used for regression fitting in order to minimize the influence of measurement artifacts. The maximum value for σ_i (Δn) was therefore less than 4% over the entire injection range used for regression fitting, and was less than 1% for $\Delta n > 10^{15}$ cm^{-3}.

4 Results

A total of 225 IDLS measurements were performed in this study both after dark annealing and after light soaking. Given the large number of IDLS measurements, it was not feasible to present an in-depth analysis of individual IDLS curves; however, we summarize key lifetime metrics and plot a few typical IDLS curves here for the benefit of the reader. After dark annealing, the lifetime of the samples (τ_{DA}) was found to range between 100 and 160 μs, with a majority of the samples displaying τ_{DA} values of 140±12 μs. τ_{LS} was found to be 73±4 μs, with the full range being 61–82 μs. This represented a decrease in lifetime due to light soaking of about 48% (±3%). J_{0e} values between 88±7 fA/cm^2 were obtained when fitted using method B, indicating a passivation quality typical of commercial PECVD SiN_x:H dielectrics applied on shallow emitters.

Figure 2 shows a typical set of lifetime curves fitted using one constrained method (method B) and one partially unconstrained method (method D) using data set from the same sample.

A number of important observations can be made from Fig. 2. First, clear evidence of BO-related CID can be observed, with τ_{LS} (red points) displaying a strong injection-dependence in lifetime compared to τ_{DA} (black points). Secondly, both τ_{DA} and τ_{LS} appear to be well-described by the lifetime components presented in Eqs. (1) and (2) respectively, evident from the good visual fit between the data (points) and model (lines), and relatively close-to-unity values for the GOF metrics (Q_{DA}, Q_{LS} and Q_{global}) for both methods.

The modeled curves (solid and dotted lines) in Fig. 2 also highlight the limiting recombination mechanisms affecting τ_{DA} and τ_{LS}. In the case of τ_{DA}, it can be seen that τ_{surf} (green dotted line) is the dominant recombination mechanism, with $\tau_{SRH,non\text{-}BO}$ (purple dotted line) and $\tau_{bulk,fixed}$ (yellow dotted line) being less limiting to overall lifetime. In contrast, τ_{LS} is primarily limited by $\tau_{SRH,BO}$ in low injection ($\Delta n < 3 \times 10^{15}$ cm^{-3}) and by τ_{surf} in high injection ($\Delta n > 3 \times 10^{15}$ cm^{-3}). This has two main implications. First, this confirms that τ_{LS} is sensitive to recombination from the BO defect over a sufficiently broad injection range, which is an important requirement for the determination of k_1 for the BO defect. Secondly, although τ_{surf} dominates lifetime in high injection for τ_{LS}, the high sensitivity of τ_{DA} to τ_{surf} ensures the accuracy of τ_{surf} when determined from τ_{DA} as in method B (dotted green line) or from τ_{LS} as in method D (solid green line).

In fact, for this particular sample, the J_{0e} obtained from fitting τ_{DA} (84.7 fA/cm^2, method B) appears to be about 4.5% higher than that obtained from fitting τ_{LS} (80.8 fA/cm^2, method D). The implications of an apparent change in J_{0e} after light soaking of the sample are discussed later, but we emphasize two points here. First, this demonstrates the utility of comparing the fits from constrained and unconstrained fitting methods to detect potential light-

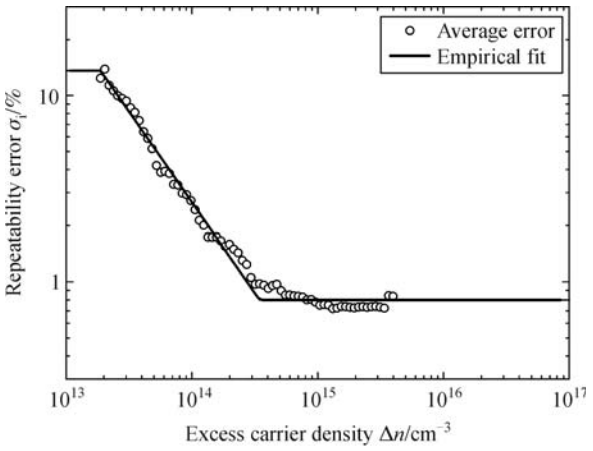

Fig. 1 Average repeatability error in inverse lifetime (circles) as a function of excess carrier density for IDLS data measured by PCD using the generalized method. Black line shows empirical fit to the data

induced changes in the sample. Secondly, it is worth noting that the failure to account for this change causes an anomalously low value for ($\tau_{LS}^{-1} - \tau_{DA}^{-1}$) in high injection ($\Delta n > 2 \times 10^{16}$ cm^{-3}).

Figure 2 also demonstrates the power of regression and appropriate GOF metrics to determine suitability of the model and methods. A cursory visual inspection would suggest that the fits to τ_{LS} for method B and D are both acceptable based on the visual overlap between red data points and lines. However, a comparison of the corresponding GOF metric, Q_{LS}, shows that method D provides a significantly better fit to τ_{LS} (Q_{LS} = 1.02) compared to method B (Q_{LS} = 2.93), the latter being noticeably higher than unity. In fact, a closer look in the high injection regime dominated by τ_{surf} ($\Delta n > 2 \times 10^{16}$ cm^{-3}) shows that the modeled τ_{LS} curve from method B (solid red line) deviates from the observed values (red squares). Although this difference may be hard to discern visually from τ_{LS}, the clear deviation of ($\tau_{LS}^{-1} - \tau_{DA}^{-1}$) from $\tau_{SRH,BO}$ from method B confirms that failure to account for changes in

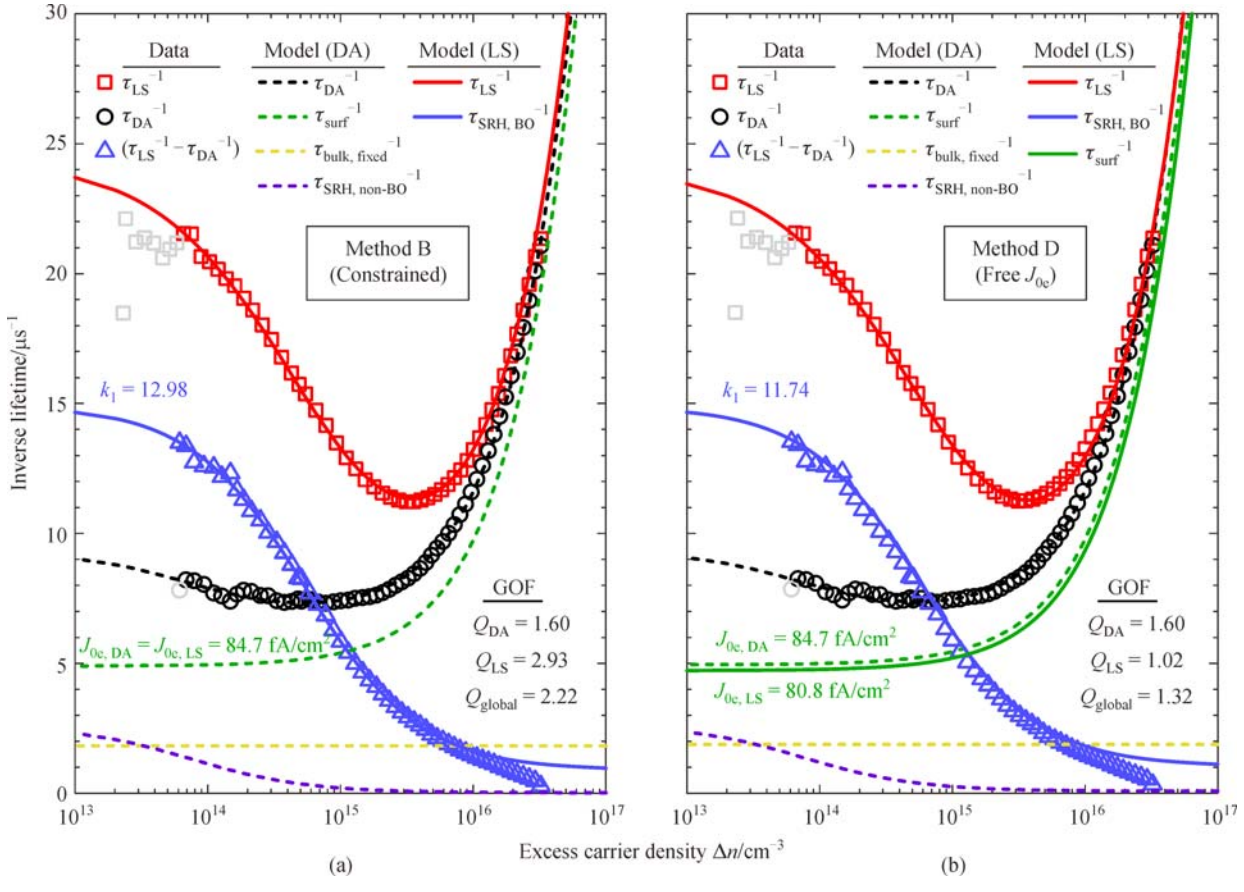

Fig. 2 IDLS data set showing measured inverse lifetime τ_{DA}^{-1} (black circles), τ_{LS}^{-1} (red squares) and ($\tau_{LS}^{-1} - \tau_{DA}^{-1}$) (blue triangles) for the same sample modeled using method B (a) and method D (b). Grey points indicate data rejected for regression. Best fits to τ_{LS}^{-1} and τ_{DA}^{-1} are indicated by the solid red line and dashed black line respectively. Fitted lifetime components are indicated by other colored lines: $\tau_{bulk,fixed}$ (yellow), $\tau_{SRH,non\text{-}BO}$ (purple), τ_{surf} (green) and $\tau_{SRH,BO}$ (blue). Components determined from τ_{DA} fitting are indicated by dashed lines. Solid lines indicate unconstrained components determined from τ_{LS} fitting. Unit-less GOF metrics for τ_{DA} fitting (Q_{DA}), τ_{LS} fitting (Q_{LS}) and overall GOF for τ_{DA} and τ_{LS} fitting (Q_{global}) are also indicated

τ_{surf} has an impact on the fitted value of k_1. This demonstrates that Q metrics with values closer to 1 are good indicators of fit quality and validates the approach presented in Section 3.3.1 to calculate Q.

Finally, it can be seen in Fig. 2 that the optimal value for k_1 that leads to the least Q_{LS} varies between methods even when the same data set is used. In the case of the presented set of measurements, k_1 varies by ~10% between methods (k_1 = 12.98 for method B and k_1 = 11.74 for method D). As will be shown later, this represents an extreme case within the data set. Nevertheless, it highlights the sensitivity of fitted k_1 to potential changes in non-BO related lifetime components and to the fitting method.

Similar fitted curves with varying fit quality and fitted parameters were obtained when other methods were used to analyze the same data set. While the subtleties relating to each of the fitting methods cannot be discussed here at length, we focus on overall trends relating to the fitting methods drawn from the large data set analyzed in this work. In particular, we present key statistical metrics and discuss results from the various fitting methods.

4.1 Goodness-of-fit for various fitting methods

As discussed in Section 3.3.1, GOF metrics provide important clues regarding the accuracy of the methods and of the assumptions behind the various methods. Since the goal here is to compare the validity of different methods, and their accuracy in modeling $\tau_{SRH,BO}$, we focus on two key GOF metrics: Q_{LS} and Q_{global}, which refer to the GOF associated with τ_{LS} fitting, and the overall GOF for τ_{LS} and τ_{DA} fitting respectively. These are plotted in Fig. 3 and Fig. 4 respectively. We note that because parameters for fitting τ_{DA} were the same for all methods except methods C, I and J, the GOF metric for τ_{DA} (Q_{DA}) was equal for methods A, B and D-H. For the sake of brevity, Q_{DA} is therefore not plotted; however, qualitative information about the GOF for τ_{DA} can be deduced from the difference between Q_{global} and Q_{LS}, and is commented upon below where appropriate. Note that the centrality and variability metrics reported in this work are the median and median absolute deviation (MAD) rather than the mean and standard deviation since the latter metrics are more sensitive to outliers and skews.

It can be seen from Fig. 3 and Fig. 4 that not all methods result in good overall fits to τ_{LS} and τ_{DA}. Constrained methods (methods A, B and C), for example, display Q_{LS} and Q_{global} values noticeably greater than 1 (Q_{LS} = 1.82–2.05, Q_{global} = 1.62–2.63). The same can also be concluded for method F, which also displays values for Q_{LS} (1.69) and Q_{global} (1.53) that are similar to the constrained methods.

These results have two implications for interpreting the Q values for other methods. First, the low GOF of methods A, B and C indicates that attempts to fit τ_{LS} using

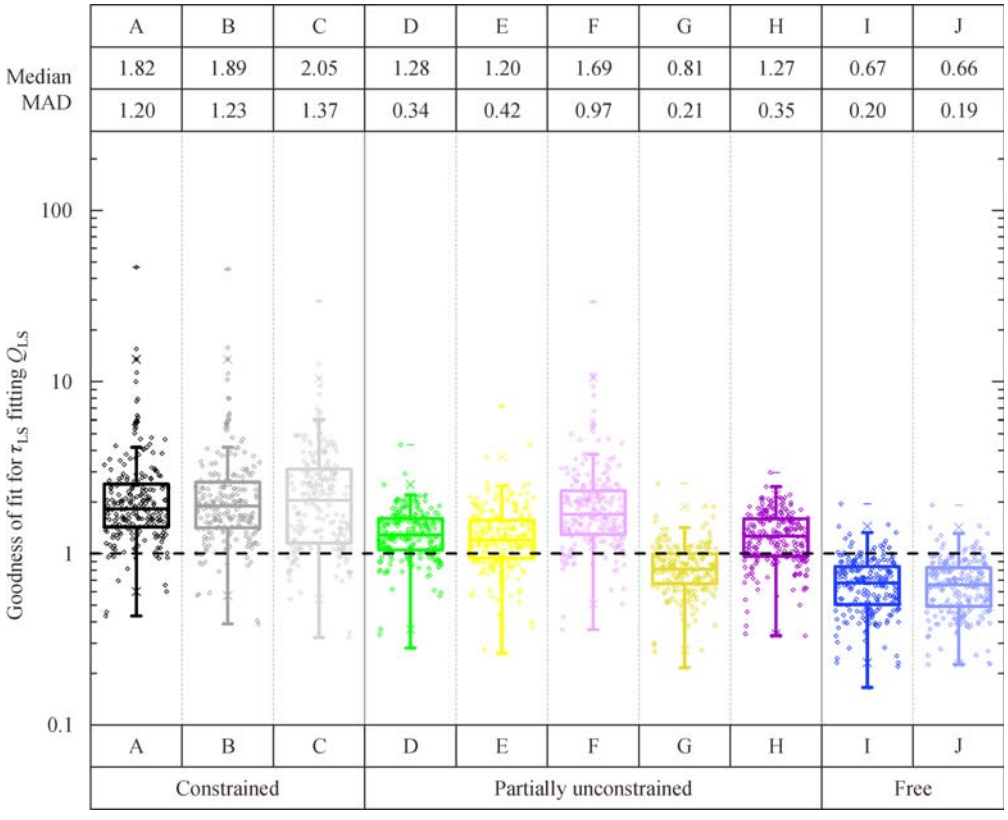

Fig. 3 Box plot of reduced Chi-square (Q_{LS}) for τ_{LS} fitted using various methods described in Table 1 (Median and MAD values of Q_{LS} are listed above plot. Dashed line at Q = 1 is shown for reference. Note that Q_{LS} is a unit-less quantity)

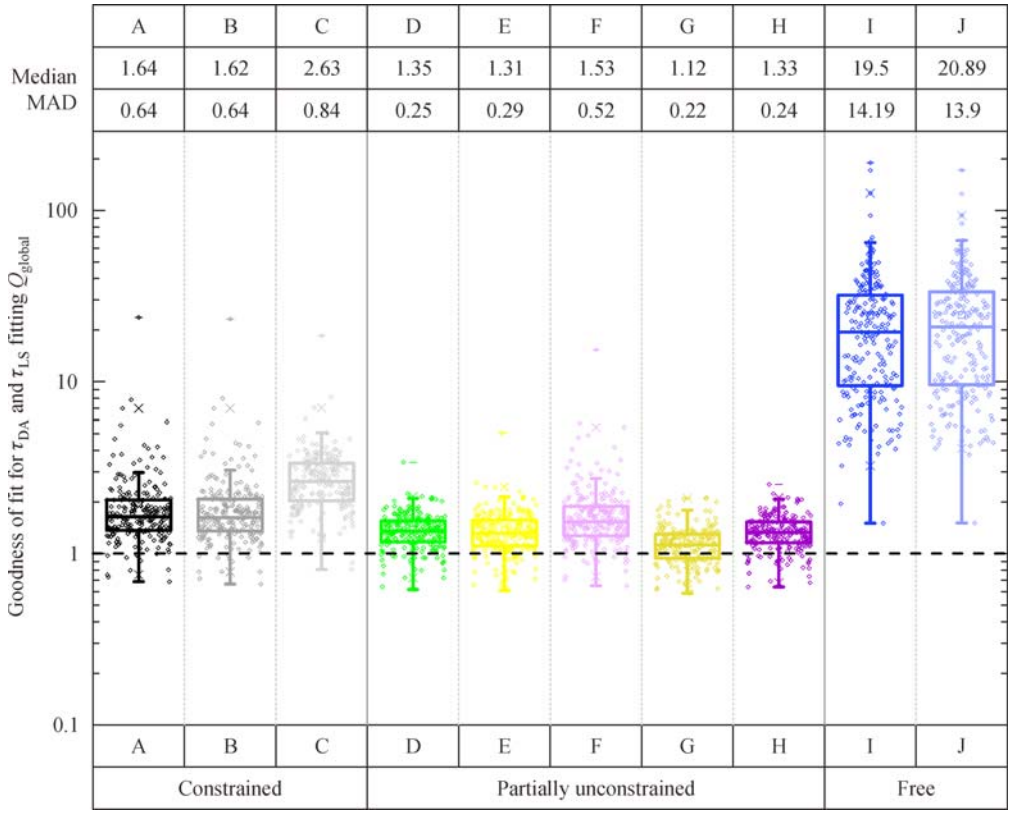

Fig. 4 Box plot of the global reduced Chi-square (Q_{global}) for fits to both τ_{LS} and τ_{DA} from the various fitting methods described in Table 1 (Median and MAD values of Q_{global} are listed above plot. Dashed line at $Q = 1$ is shown for reference. Note that Q_{global} is a unit-less quantity)

parameters obtained from τ_{DA} fitting (τ_{surf}, $\tau_{bulk,fixed}$ and $\tau_{SRH,non\text{-}BO}$) result in poor fits. Secondly, the poor fitting to method F, indicated by high Q_{LS} and high Q_{global} demonstrates that $\tau_{SRH,non\text{-}BO}$ is not affected by light soaking. Thus, other methods that rely on these assumptions are also unlikely to be accurate. Such is the case with method H (free τ_{surf} and $\tau_{SRH,non\text{-}BO}$), which displays lower Q_{LS} (1.27) and Q_{global} (1.33) but relies on the inaccurate assumption that $\tau_{SRH,non\text{-}BO}$ is impacted by light soaking.

Similarly, methods I and J display excellent fits to τ_{LS} ($Q_{LS} \sim 0.66$). However, interpreting this as a simultaneous change in all non-BO lifetime components due to light soaking would be inaccurate. Instead, the low Q_{LS} values, which are noticeably less than 1, are an indication that these methods 'over-fit' τ_{LS} data owing to the large degrees of freedom (free parameters) available for fitting τ_{LS} data. Moreover, when $\tau_{SRH,\ BO}$ is subtracted from τ_{LS} to obtain τ_{DA} for methods I and J, this results in extremely poor fits to τ_{DA} as demonstrated by the high Q_{global} values of ~20. While not plotted, the poor fits using methods I and J could be confirmed visually. Thus, methods I and J can also be ruled out as being inaccurate. This also rules out the possibility that fitting to τ_{LS} alone can accurately determine the lifetime components defining τ_{DA}.

Methods D (free τ_{surf}) and E (free $\tau_{bulk,fixed}$), on the other hand, display Q values close to 1 (Q_{LS} = 1.31–1.35, Q_{global} = 1.20–1.28). These are noticeably lower than the constrained methods and also lower than method F. This suggests that either τ_{surf} or $\tau_{bulk,fixed}$ could be affected by light soaking. It may also be possible that both of these components are affected, as indicated by the low Q_{LS} (0.81) and Q_{global} (1.12) for method G. However, since the Q_{LS} value for method G is less than 1, the issue of over fitting cannot be ruled out. Thus, of the various methods tested, methods D, E and G — in that order — are most likely to be accurate.

4.2 Impact of fitting methods on k_1

While GOF metrics help to identify inaccurate methods, methods with comparable Q_{LS} or Q_{global} that are close to unity may not necessarily all be accurate. This could be caused, for example, by the regression algorithm attempting to adjust k_1 in order to achieve a better GOF (lower Q values) — but at the expense of accuracy. Hence, it is instructive to consider the fits to k_1 resulting from the various methods, which are plotted below in Fig. 5.

We first discuss the variability of fitted k_1 (MAD) between methods as this is particularly important for

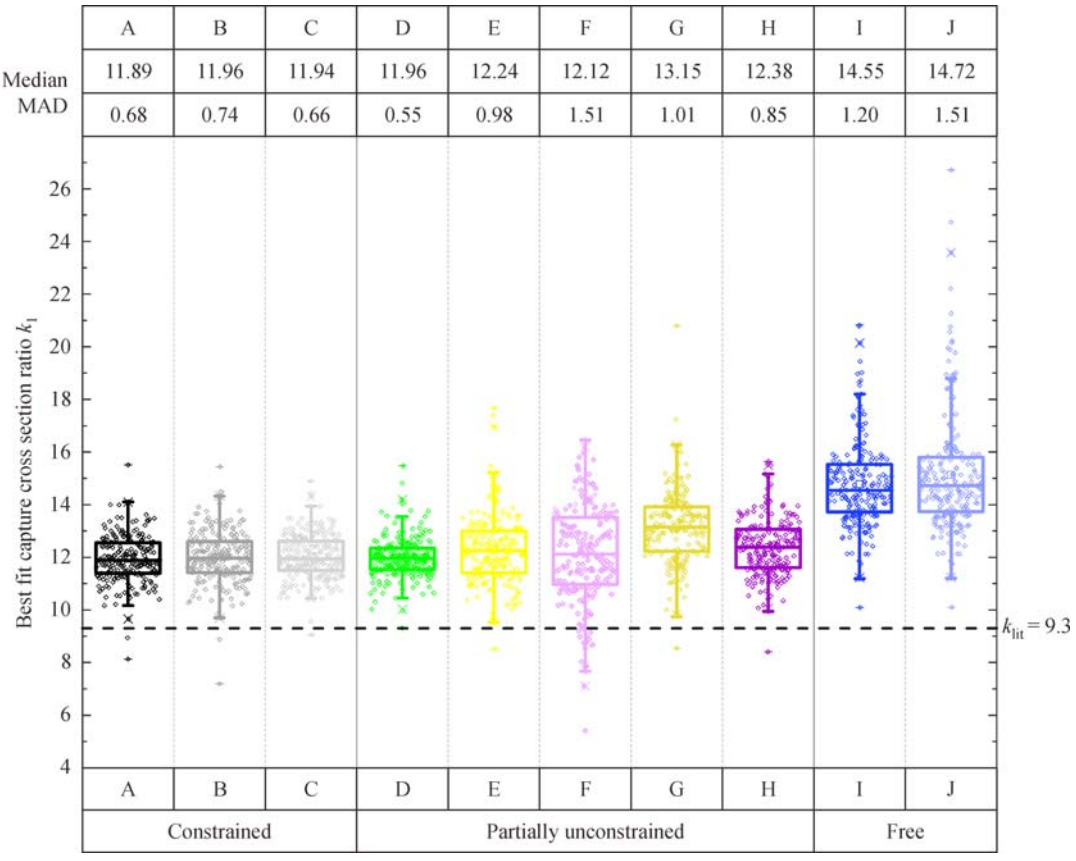

Fig. 5 Box plot of best fit capture cross section ratio (k_1) obtained using the fitting methods listed in Table 1 (Median and MAD of k_1 for each method are listed above the plot. k_1 value from the literature (k_{lit}) based on TDLS measurements [6] is denoted by red line)

evaluating the accuracy of the methods. In particular, methods which cause k_1 to be adjusted to account for inaccuracies in other lifetime components can be expected to display higher MAD in k_1 compared to more accurate methods.

This is apparent when comparing Fig. 4 and Fig. 5. It can be seen that unconstrained methods which display high MAD in Q_{global} (methods F, I and J) also display a correspondingly high MAD in k_1. Once the higher median Q_{global} for these methods is also considered, it is clear that k_1 values for these methods were indeed influenced by attempted changes in other fitting parameters to achieve the best possible GOF. Similarly, constrained methods (methods A, B and C) also display moderately high MAD values for both Q_{global} as well as k_1.These results confirm the inaccuracy of the assumptions underlying the constrained methods (A, B and C) as well as some of the unconstrained methods (F, H, I and J).

Comparing the MAD in k_1 also helps distinguish between unconstrained methods with low Q_{global} (methods D, E, and G). It can be seen that despite comparable Q_{global} values (1.12–1.35), these methods display different MAD in k_1, with methods E (0.98) and G (1.01) displaying almost twice as much MAD in k_1 as method D (0.55). Note that the MAD in k_1 of method D is also the least of all methods tested. This strongly suggests that the assumption underlying method D (changing τ_{surf}) more accurately reflects the changes due to light soaking than that underlying method E (changing $\tau_{bulk,fixed}$). However, since method G results in lower Q_{LS} and Q_{global} than both methods D and E, a combined change in τ_{surf} and $\tau_{bulk.fixed}$ cannot be ruled out.

The comparison of GOF and MAD in k_1 therefore suggests than method D is the most accurate modeling method, with method G possibly also being accurate. These results not only confirm that light soaking causes changes in lifetime components other than $\tau_{SRH,BO}$, but also confirm that these changes can be successfully modeled by allowing τ_{surf} (and possibly also $\tau_{bulk,fixed}$) to change.

Comparison of the fitted k_1 between methods also leads to a few other interesting observations. First, it can be seen that the median k_1 ranges from 11.89 to 14.72 between methods. This clearly shows that different methods lead to noticeable different k_1 values.

Secondly, k_1 for individual samples for a given method are significantly different. For example, even for the method with the least variability in k_1 (method D), k_1

ranges from 11 to 13 (excluding extreme outliers). This represents a maximum deviation of 8% from the median. For the method with the largest variance (method F), k_1 deviates 35% from the median. This demonstrates the importance of using large data sets to determine k_1, particularly for IDLS data.

Further, when comparing median k_1 values between methods are compared, it can be seen that inaccurate methods either over- or under-estimate k_1. Compared to the most accurate method (method D, k_1 = 11.96), other unconstrained methods display either significantly higher k_1 (methods I and J, k_1 = 14.55–14.72) or moderately higher k_1 (methods E, F and H, k_1 = 12.12–12.38). In contrast, the constrained methods display either lower or comparable median k_1 values (11.89–11.96).

As previously mentioned, this is likely the result of the regression algorithm attempting to change k_1 in order to compensate for inaccurate parameter values for other lifetime components. Higher k_1 values are indicative of an overestimation in the change in $\tau_{bulk,fixed}$ (methods E, F, I and J), or an overestimation in $\tau_{SRH,non\text{-}BO}$ (methods F, H, I and J). Similarly, an overestimation of τ_{surf} in the case of the constrained methods (methods A, B and C) could lead to an underestimation in k_1.

Note that although it is possible that changes in components other than τ_{surf} do occur, or that no changes other than $\tau_{SRH,BO}$ occur due to light soaking, the poor overall GOF for the inaccurate methods suggests that these changes are either restricted to individual samples or are negligible.

Finally, based on a reduced data set consisting of 208 measurements with outliers rejected, the final median and MAD of k_1 using method D was determined to be 11.90±0.45 (11.91±0.57 using the average and standard deviation).

4.3 Changes in non-BO related lifetime components

A careful analysis of the GOF in various injection ranges (not plotted) confirmed an injection-dependent change in lifetime, particularly in high injection, that can be modeled well by either allowing for changes in τ_{surf} alone (as in method D) or in both τ_{surf} and $\tau_{bulk,fixed}$ (as in method G). We first consider changes in τ_{surf}. Since method B does not involve a changing τ_{surf} component, the relative difference in fitted J_{0e} from methods B and D represents the percentage change in J_{0e} due to light soaking. If changes in J_{0e} were due to the random errors in fitting, they would be expected to display a roughly normal distribution centered at 0%; however, our analysis showed that this relative change in fitted J_{0e} due to light soaking ranged from –10% to + 5%, with ~75% of the samples undergoing a decrease in J_{0e} due to light soaking. Similarly, when method G was used, the relative change in fitted J_{0e} ranged from –8% to + 1%, with ~90% of the samples displaying a decrease in J_{0e} due to light soaking. In both cases, the apparent light-induced change in J_{0e} displayed a roughly normal distribution but was centered at roughly –1.5% rather than 0%. This represents an average light-induced decrease in fitted J_{0e} of roughly 2 fA/cm^2. Although this change is less than the average deviation in J_{0e} between samples, this effect was statistically significant when compared to the uncertainty in J_{0e} estimation. In the case of the data set presented in Fig. 2, the difference in fitted J_{0e} between methods B and D is ~4 fA/cm^2, which is higher than the median decrease in J_{0e}, but well within the range observed across the data set.

Similarly, when illumination-induced changes in $\tau_{bulk,fixed}$ were analyzed by comparing fits from methods G, a majority of the samples (89%) appeared to display a decrease in fitted $\tau_{bulk,fixed}$ due to light soaking rather than an increase, with a distribution in apparent light-induced change in $\tau_{bulk,fixed}$ ranging from –60% to + 20% with a peak at roughly –35%. This corresponds to an average apparent light-induced decrease in $\tau_{bulk,fixed}$ of ~200 μs. Despite the seemingly large value, the small contribution of $\tau_{bulk,fixed}$ to overall recombination (as seen in Fig. 2) suggests that the inherent uncertainty in parameter fitting is quite large for $\tau_{bulk,fixed}$. This explains why the GOF for method G is only marginally better than method D in spite of allowing for large changes in $\tau_{bulk,fixed}$ (±20%). Nevertheless, the fact that the decrease in $\tau_{bulk,fixed}$ is statistically significant suggests this may be a real effect.

Finally, in contrast to τ_{surf} and $\tau_{bulk,fixed}$, attempting to model potential changes in $\tau_{SRH,non\text{-}BO}$ (from methods F and H) did not display any clear statistically meaningful trends.

5 Discussion

The results above highlight four important points. First, it is clear that assuming $\tau_{SRH,BO}$ to be the only variable parameter between τ_{DA} and τ_{LS} fitting — in other words, assuming light soaking only causes a change in $\tau_{SRH,BO}$ — is most likely an inaccurate assumption for the samples used in this work. Further, light soaking appears to cause noticeable changes in lifetime at high injection (attributable to changing τ_{surf}) and may also be causing minor and apparently injection-independent changes (modeled in this work by changing $\tau_{bulk,fixed}$).

Secondly, the results show that allowing the wrong fitting parameters to vary does not necessarily improve the variability of fitted k_1. Thus, not all methods to determine k_1 are accurate. Thirdly, considering the variability in k_1 for a given method, it is clear that the use of smaller IDLS data sets to determine k_1 can be error-prone.

Finally, median values of k_1 for all fitting methods are significantly different from the oft-quoted value of 9.3 obtained from a combination of method A and TDLS analysis [6]. In fact, only outliers in this study produced fits to $k_1 \leqslant 10$ for any of the methods used in this study. We

now discuss the implications of these results in detail in the following sections.

5.1 Influence of modeling methods on k_1

The median k_1 of 11.9 for method A in this study is significantly different from a majority of the reported values in the literature using the same methods for the fully formed BO defect. Statistical tests confirm that k_1 values from method A in this study are greater compared to other reported values of 8.3 [5], 9.3 [6] and 9.9 [13] with 95% confidence. Finally, only one reported k_1 value of 12.1 [10] (using method B) appears to correlate well with the results in this study.

There are multiple possible reasons why values in this work differ significantly from previous work; however, we focus here on the influence of modeling methods. An important point to note is that none of the other studies thus far have used large data sets of similar samples and therefore values reported in those studies have an inherent degree of uncertainty that may be larger than the statistical variability reported in this work. This could be caused by the use of samples with different concentrations of the BO defect (for example due to varying N_A [4] or degree of compensation [8,11]) or different overall lifetime, both of which may cause differences in the regression uncertainty for k_1. Moreover, GOF metrics were not quantified in some studies [5,8,13], making it difficult to assess the models used and therefore the accuracy of fitted k_1 values. Thus, it is possible that the lower fitted values of k_1 in previous studies are due to limited sample sizes.

Secondly, a number of studies employing method A have ignored IDLS data in high injection where τ_{DA} appears to be greater than τ_{LS}, which results in negative values for $(\tau_{LS}^{-1} - \tau_{DA}^{-1})$ [4,6]. Since such data cannot be accurately fitted without accounting for potential light-induced changes in τ_{surf}, it may have been more correct to use method D in such cases. Further, the lack of a diffused emitter in prior work may have resulted in larger changes in τ_{surf} than seen in this work. Accounting for such changes using method D would have most likely resulted in larger k_1 values and therefore closer to the values reported in this work.

The impact of a diffused emitter on k_1 fitting is also highlighted in the case of Ref. [10], in which k_1 determined from an emitter-diffused p-type wafer was found to be 12.1 using method B. This is not only closer to the value of 11.9 determined in this work but is also significantly different from k_1 values of 10 or less reported for p-type wafers without an emitter diffusion [4–6,13]. The presence of an emitter is also expected to increase J_{0e}, and therefore it is possible that fitted k_1 is related to high J_{0e} values rather than the presence of an emitter. This possibility is further discussed in Section 5.2 below.

Finally, when methods I or J is used, fitted k_1 in this work appears to be significantly lower (k_1 = 14.5 to 14.7) compared to a reported value of 19.3 [14] for those methods. However, we note that explicit modeling of $E_{trap,2}$ in the latter work could have led to the higher k_1 value reported. We comment further on this in Section 5.5. Nevertheless, the latter result does confirm that the use of methods I and J can lead to larger k_1 values than methods A and B.

5.2 Influence of sample type and measurement methods on k_1

Based on the comparison to reported k_1 values from the literature, it is evident that modeling methods could influence the determination of k_1 and can explain some of the inconsistencies in reported k_1. However, the noticeably larger values of k_1 from this work and in Refs. [10] and [14] suggests other underlying causes. One possible explanation is that k_1 values determined in this work are specific to the wafers used in this study. For example, the commercial p-type wafers used in this study contained other SRH defects beside BO. Although these defects were confirmed not to cause CID, they necessitated the use of the $\tau_{SRH,non\text{-}BO}$ component to achieve good fits to τ_{DA}. Attempting to solve for two SRH defect components ($\tau_{SRH,BO}$ and $\tau_{SRH,non\text{-}BO}$) simultaneously during τ_{LS} fitting, as in methods I and J, resulted in low-Q, but inaccurate fits. This issue may be less relevant in wafers that do not contain defects other than BO, such as the p-type float-zone silicon wafers fitted with method J in Ref. [14].

Further, in the single study where k_1 was found to be similar to that determined in this work, the wafers used included an emitter diffusion step [10]. This is similar to the wafers in this study and unlike the wafers used in other studies with comparable N_A values [4,6]. The use of a shallow emitter for lifetime characterization, such as that used in this study, may have either have a neutral or negative influence on the accuracy of k_1 estimation. On the one hand, wafers with emitter diffusion are known to display DRM [28], which artificially increases the measured lifetime in low injection. Hence, this is expected to lead to a reduction in the fitted k_1. While this was the case with some samples in this study, the effect was found to be small as excluding these samples did not appear to appreciably change the median k_1. Moreover, DRM effects do not explain why k_1 values in this work are higher, rather than lower, compared to other work on samples without emitters.

Another potential drawback of using emitter-diffused samples is that an emitter with a high J_{0e} (low τ_{surf}) may reduce the injection range in which $\tau_{SRH,BO}$ (and therefore k_1) is sensitive to model fitting. It is likely that a more lightly diffused emitter or better surface passivation would have increased the injection range in which $\tau_{SRH,BO}$ is the limiting component of lifetime in τ_{LS} (see Fig. 2). Considering that k_1 appears to be highly sensitive to

light-induced changes in J_{0e} in the samples used in this work, the question arises whether lower overall J_{0e} in the samples could lower the fitted k_1. However, a detailed analysis on our data set revealed that even the best passivated samples in this study ($J_{0e} \approx 75$ fA/cm^2) displayed a similar range of fitted k_1 values as the worst passivated samples ($J_{0e} \approx 100$ fA/cm^2). Moreover, no discernible correlation could be found between k_1 and the absolute value of the fitted J_{0e} despite a strong correlation between k_1 and light-induced changes in J_{0e}. While this does not rule out the influence of absolute J_{0e} on the fitted k_1 for samples with J_{0e} lower than that seen in this study, we point out that this is unlikely to be the case. Nevertheless, the possibility of emitter diffusion skewing the fitting of k_1 is a topic worthy of further investigation.

On the other hand, the presence of an emitter could also be beneficial since an emitter is expected to reduce the impact on lifetime of light-induced changes near the silicon-dielectric interface. This is because τ_{surf} is a lumped parameter that accounts for recombination in the emitter as well as from the surface. Thus, the absence of an emitter may increase τ_{surf} (i.e. reduce J_{0e}), but would also make τ_{surf} more sensitive to potential light-induced changes at the silicon-dielectric interface and to any non-homogeneities at the surface (e.g. surface damage). We also note that the emitter diffusion step is a necessary process in solar cell fabrication. Hence, even in the unlikely case that diffused emitters play a role in k_1 fitting, the k_1 values determined in this work remain highly relevant to the characterization of BO defects in commercial p-type solar cells and precursors. The large data set used in this work provides further statistical confidence in the fitted k_1 values in this work.

Finally, we note that fitting of k_1 may also be influenced by the measurement technique used to obtain IDLS data. The use of photoluminescence (PL) lifetime spectroscopy to determine k_1 [10] could, for example, eliminate the influence of DRM, if present. Therefore, PL spectroscopy may be better suited for characterizing BO defects in p-type samples with heavily doped emitters. Nevertheless, both PCD and PL techniques are sensitive to edge recombination and carrier trapping effects, which may either cause an increase or decrease in fitted k_1 depending on the sample type and the range of injection levels considered for analysis.

5.3 Apparent changes in non-BO related lifetime components

The statistically significant changes in lifetime components not modeled by $\tau_{SRH,BO}$ in this study point to either underlying physical reasons for light-induced changes in τ_{surf}, and to a smaller extent in $\tau_{bulk,fixed}$, or indicate deficiencies in the model describing $\tau_{SRH,BO}$ that led to apparent changes in τ_{surf} and $\tau_{bulk,fixed}$. We first consider possible physical mechanisms for such changes.

Illumination-induced changes in τ_{surf} have been observed in other studies [32–35] and are thought to be related to charge trapping in the dielectric layer [33,35]. Such effects could lead to an improvement in surface passivation when SiN_x:H layers are deposited on a diffused n-type surface (as is the case in this study). This could explain the light-induced reduction in J_{0e} seen in a majority of the samples in this study, while a varying magnitude of the charge trapping effect could help explain the distribution of differences in fitted J_{0e} between methods B and D. Likewise, the small increase in J_{0e} observed in some samples could either be due to small uncertainties in the fitted parameters, or due to minor surface damage induced during wafer handling. However, the presence of an emitter is expected to make τ_{surf} less sensitive to such changes reduce the impact of such damage on the observed J_{0e}.

Although samples in this work largely display a decrease in J_{0e} due to light soaking, it is important to consider that a statistically significant increase in J_{0e} due to light-soaking could occur in other sample types. For example, the charge trapping effect in SiN_x:H that improves τ_{surf} on emitter-diffused p-type wafers may have a negative or neutral effect on τ_{surf} on p-type wafers without an emitter, or on wafers passivated using a different dielectric. In addition, samples without an emitter may be more susceptible to changes in τ_{surf} due to surface damage. In fact, there may be some evidence of this in early studies [4–6] wherein an additional shallow trap level at roughly $E_V + 0.15$ eV was found to be required to fully describe the high-injection behavior of p-type wafers without an emitter. Interestingly, not all wafers were found to require this trap level. This is particularly relevant since our attempts to model a small increase in J_{0e} using an SRH defect revealed that a minor increase in J_{0e} of 4 fA/cm^2 could be effectively modeled by a shallow defect located in a narrow range between $E_V + 0.05$ eV and $E_V + 0.2$ eV. Thus, when IDL data are fitted using method B, a sample displaying an increase in J_{0e} would appear to require the shallow defect level, whereas samples with no change (or a decrease) in J_{0e} would appear not to require this level. Further, the lack of an emitter diffusion would be expected to make the samples in the other studies even more sensitive to changes in τ_{surf} than samples used in this study. As discussed in Section 5.2, any potential increase in J_{0e} between τ_{DA} and τ_{LS} in such studies could also affect the fitted value of k_1. While further studies are required to understand this effect, the results in this work suggest that accounting for potential changes in τ_{surf} due to light soaking (methods D or G) is a more accurate approach to IDLS modeling.

On the other hand, physical reasons for the apparent decrease in $\tau_{bulk,fixed}$ between τ_{DA} and τ_{LS} are harder to justify. The samples in this study were confirmed to have negligible quantities of iron and no other known CID causing defects with the exception of the BO defect. In any case, most known CID-causing defects such as iron and copper are known to display a significant injection

dependence and therefore would not be expected to cause changes in, which is assumed to be injection independent. The minor changes in $\tau_{bulk,fixed}$ observed from the analysis of method G therefore point to a deficiency in the model used to describe $\tau_{SRH,BO}$. As previously noted, Eq. (3) used to describe $\tau_{SRH,BO}$ does not include the recombination due to $E_{trap,2}$, the acceptor level of the BO defect [3,11]. The additional recombination introduced by $E_{trap,2}$, if largely injection-independent, could manifest as a decrease in $\tau_{bulk,fixed}$ and therefore explain the improved fit obtained from method G.

To check if $E_{trap,2}$ could explain the apparent decrease in $\tau_{bulk,fixed}$, an additional SRH lifetime component described by Eq. (4) was used to represent $E_{trap,2}$. This model was then used to analyze some of the curves in the data set in lieu of a variable $\tau_{bulk,fixed}$ component in method G. However, since allowing k_2 and k_1 to vary would allow any value of $E_{trap,2}$ in the lower half of the bandgap to replicate the roughly injection-independent effect modeled by $\tau_{bulk,fixed}$, two constraints were applied. First, k_1 was not allowed to vary and was fixed to the value determined using method G and applying the single defect model (Eq. (4)). Secondly, only values of $E_{trap,2}$ that required less than unity values of k_2 were considered. Preliminary results indicate that only for $E_{trap,2} > E_V + 0.2$ eV was the latter condition satisfied. Further, upper limits of k_2 for reported acceptor levels from the literature could be determined. The upper limit of k_2 was found to be 10^{-1} to 10^{-2} for $E_V +$ 0.26 eV [9,11] and 10^{-3} to 10^{-4} for $E_V + 0.35$ eV [3]. These limits largely agree with other IDLS studies incorporating the $E_{trap,2}$ level at $E_V + 0.26$ eV, which report k_2 to be roughly 2×10^{-3} [11,14]. The higher k_1 values resulting from method E and G relative to method D also suggest a minor influence of the acceptor trap level, since a decrease in such apparent injection-independent lifetime would require larger k_1 values to provide good fits to the data [14]. Thus, it would appear that the apparent changes in $\tau_{bulk,fixed}$ could be explained by the recombination activity of $E_{trap,2}$.

However, similar efforts to model changes in τ_{surf} from method D by incorporating $E_{trap,2}$ via an additional SRH defect and keeping k_1 fixed were not successful. This is because as long as other lifetime components are fixed, introducing an additional SRH component in the model only allows for a net decrease in lifetime to be modeled. However, a large majority of the samples in this study actually displayed a decrease in fitted J_{0e} and therefore an apparent net increase in surface/emitter lifetime. In fact, for some samples, τ_{LS} was actually found to display a higher lifetime compared to τ_{DA}, leading to negative values for $(\tau_{LS}^{-1} - \tau_{DA}^{-1})$, particularly in high injection ($\Delta n > 10^{16}$ cm^{-3}). Similar negative values for $(\tau_{LS}^{-1} - \tau_{DA}^{-1})$ are also alluded to in other studies on the fully formed BO defect [4–6]; however, these have largely been rejected for the fitting of k_1 in such studies. Nevertheless, it must be acknowledged that this does not rule out the possibility of explaining some, but perhaps not all, of the decrease in lifetime associated with a changing J_{0e} component using $E_{trap,2}$.

While further work is required to clarify the impact of $E_{trap,2}$, we conclude for now that there is indirect evidence of a real, but minor light-induced change in J_{0e} for the samples in this study. In contrast, the minor apparent change in seen in most samples is most likely related to $E_{trap,2}$ rather than due to an underlying change in the background lifetime. Attempts to model the data set in this study using a more accurate, two-level description of $\tau_{SRH,BO}$ [11,14,36] are currently underway to clarify these effects.

5.4 Influence of fast and slow degradation effects on k_1

It must be recognized that the conclusions regarding the validity of the modeling methods presented in this work are not only specific to the single defect model used (Eq. (4)), but also to the analysis of the fully formed BO defect in p-type silicon. As mentioned earlier, BO-related CID occurs in two stages, which appear to require very different capture cross section ratios to accurately model their impact on carrier lifetime. In the case of p-type silicon, carrier lifetime after complete formation of the BO defect in p-type silicon is largely limited by the slow forming BO defect, which can be fitted by a mid-gap defect with a capture cross section ratio similar to that determined in this study (k = 9 to 19) [4–6]. This property has been used in this work and in a majority of other studies on p-type silicon to determine k_1 and $E_{trap,1}$ assuming a single defect model with a single trap level. However, a sufficiently large contribution to the lifetime after complete degradation from the fast-forming defect (k = 65 to 100) [7,37] could result in a higher fitted value for k_1 [14].

Due to the lack of time-resolved data during the light soaking process, it was not possible to verify if the higher k_1 value of ~12 reported in this work and in Ref. [10] could be due to greater contribution to lifetime from the fast-forming defect compared to other studies reporting a lower k_1 value. However, we note that it is unlikely that the samples in this study or in Ref. [10] are significantly more influenced by the fast forming defect compared to other studies. First, the Cz samples used in this study and in Ref. [10] appear to be of similar quality and have N_A values that are well within the range studied in other works that report lower k_1 values [4–6]. Thus, differences in the net doping-normalized concentration of BO defects are likely to be minimal between the various studies. Moreover, any potential differences in the fraction of BO defects undergoing fast and slow degradation [9,14] are also expected to be minimal between this work and other studies on non-fired samples. We also note that dark annealing was performed at the same temperature (200°C) in this and other work. Unless there are other unknown factors that could increase the contribution of the fast defect center to

the lifetime after complete formation of the defect, the improved estimate of k_1 presented in this work is still valid for single-defect modeling of the fully formed BO defect in commercial p-type silicon.

Nevertheless, accounting for the influence of the fast and slow degradation centers in the fully formed defect could well lead to more accurate estimates of k_1 than that determined in this study. The exact approach to account for the influence of the fast and slow degradation centers is currently a matter of debate [9,12,14]; however, eliminating the influence of either the slow or fast forming defect has been shown to simplify analysis [5]. Time-resolved IDLS measurements leading to complete degradation such as that performed in Refs. [11,14,37] are expected to lead to more accurate estimates of k_1.

5.5 Approaches to modeling $E_{trap,2}$ in p-type silicon

Ignoring $E_{trap,2}$ has been justified in this and prior work on fully formed BO defects in p-type silicon considering the minimal additional injection-dependence in carrier lifetime introduced by the acceptor level as noted in Section 5.3 and in Ref. [7]. However, $E_{trap,2}$ is known to be dominant and non-negligible in compensated n-type material [8,11] and may have implications for the determination of k_1 in p-type silicon as well [14]. There also appears to be some evidence that $E_{trap,1}$ and $E_{trap,2}$ are related to the slow and fast degradation centers [14,38], further complicating the analysis of $E_{trap,1}$ and $E_{trap,2}$ in fully degraded p-type silicon. We briefly discuss these implications here and outline the challenges in characterizing $E_{trap,2}$ in p-type silicon.

As noted earlier, the exact location of $E_{trap,2}$ within the bandgap is not known with certainty. A recent DLTS study on p-type silicon has suggested an acceptor trap level at $E_V + 0.35$ eV; however, this was based on preliminary results and there appears to be some ambiguity in the DLTS data regarding $E_{trap,2}$ that requires further analysis [3]. In contrast, IDLS characterization of compensated n-type material has suggested a trap level at $E_V + 0.26$ eV [9,11], although $E_V + 0.15$ eV has also been shown to result in acceptable visual fits in such material [8]. While it is suspected that the estimates of $E_{trap,2}$ from compensated n-type silicon may not apply to p-type silicon due to differences in the charge state of the defect between the two material types [9], a good fit to τ_{LS} in p-type silicon has nevertheless been achieved [14]. Even so, the absence of a comprehensive analysis via TDLS or DLTS makes it difficult to establish $E_{trap,2}$ unambiguously in p- and n-type material.

Compounding the situation further is the fact that the capture cross section ratio associated with $E_{trap,2}$ (k_2) also appears to vary widely between studies. k_2 has been variously reported in p-type silicon as 1.5×10^{-2} [9], 2.1×10^{-3} [14] and 2.55×10^{-3} [11] for $E_{trap,2} = E_V + 0.26$ eV, and simply as $k_2 << 1$ for $E_{trap,2} = E_V + 0.15$ eV [4]. In contrast, k_2 in compensated n-type silicon is reported to be 6×10^{-2} for $E_{trap,2} = E_V + 0.15$ eV [8] and 2.55×10^{-3} [11] for $E_{trap,2} = E_V + 0.26$ eV. k_2 has not been estimated to date in p- or n-type silicon for $E_{trap,2} = E_V + 0.35$ eV (the trap level estimated from the DLTS study [3]).While estimates of k_2 all indicate that k_2 is $<< 1$, the uncertainty in k_2 is considerable. A large part of this uncertainty stems from the fact that the injection dependence attributable to $E_{trap,2}$ is not very sensitive to k_2 [11]. The varying choice of $E_{trap,2}$ further compounds this effect since there could exist multiple combinations of E_{trap} and k to describe the injection-dependent behavior of any given defect. Moreover, if $E_{trap,2}$ is specific to either the fast or slow recombination centers, then k_2 may also be a function of the charge state of the defect at $E_{trap,2}$, and therefore the substrate doping type [9]. Finally, the uncertainty in k_2 could be related to the assumed value of k_1. We note that most attempts to determine k_2 within a two-level defect model have assumed k_1 to be in the range of 9–10 [8,11,12]; however, since this value of k_1 was itself determined using a single defect model with a single trap level (Eq. (4)) such as that used in this study, the resulting estimates of k_2 may be inaccurate. All these reasons make it particularly difficult to study $E_{trap,2}$ using data from the fully formed BO defect in p-type silicon, in which the slow degradation center appears to dominate.

Thus, in order to investigate $E_{trap,2}$ in p-type material using a two-level defect model, it may be necessary to not only distinguish between the fast and slow degradation effects, but also to solve for all unknowns describing $\tau_{SRH,BO}$ (k_1, k_2, $E_{trap,2}$, τ_{n0} and τ_{p0}) simultaneously. While the issues regarding fast and slow degradation can be solved via time-resolved measurements of τ_{LS} [11,14,37], the disambiguation of parameters defining $\tau_{SRH,BO}$ within a two-level defect model cannot be easily resolved. This is primarily because the effective DOF associated with fitting $\tau_{SRH,BO}$ using data from a single sample type is lower than the number of variables to be solved. However, analyzing samples containing variations in N_A [9,11], in sample temperature (via DLTS or TDLS) or potentially isolating the recombination activity of $E_{trap,2}$ or $E_{trap,1}$ (as suggested in Ref. [14]) are all approaches that could simplify parameterisation or reduce the number of unknown parameters.

Attempts to perform regression on the current data set using a two-level defect model are currently underway to check if statistically variation could help establish a likely range of fit parameters.

5.6 Implications for lifetime characterization of CID defects

The potential invalidity of the assumption that light soaking causes changes only in $\tau_{SRH,BO}$, has significant implications for the determination of other SRH recombination characteristics of the BO defect. In particular, changes in τ_{surf} are expected to result in an over- or under-

estimation of normalized defect density [5] and introduce additional uncertainty in the determination of the BO defect state transition kinetics [39], both of which rely on IDLS measurements.

These effects are expected to be even more important for TDLS analysis, which relies on determining the temperature dependence of $\tau_{SRH,BO}$. All TDLS studies done on BO defects so far have determined recombination properties based on the temperature dependence of τ_{LS} [6] or τ_{DA} [15] rather than $\tau_{SRH,BO}$ alone. If the temperature dependence of τ_{surf} [40] compensates that of $\tau_{SRH,BO}$, and changes in τ_{surf} in those studies were non-negligible, this could have resulted in an under- or over-estimation of k_1 and $E_{trap,1}$. However, since the analysis was restricted to low injection conditions in those studies, the degree of uncertainty introduced due to changing τ_{surf} is expected to be small. Nevertheless, this effect may be non-negligible for TDLS analysis at higher injection levels or for the analysis of shallower trap levels such as the acceptor level of the BO defect ($E_{trap,2}$).

Although BO defects are the primary focus in this work, these effects are expected to be equally relevant for the characterization of other similar SRH defects such as the CID defect in multi-crystalline silicon [41], which may be particularly vulnerable to changes in τ_{surf} due to the long annealing and illumination exposure times required to cause defect state transitions.

Finally, the fitting methods used in this study could be useful for modeling of lifetime data involving SRH defects in general, as well as other types of data sets that require nonlinear regression. In particular, the robust, unit-less measure for goodness of fit used in this work offers an improvement over visual fitting or mean-squared-error based metrics with arbirary units used in previous studies. As demonstrated in this work, a reduced Chi-square metric accounting for repeatability error not only allows for easy interpretation of the fit quality but could also be used to compare fitting results from data sets measured using the same measurement tool. Additionally, accounting for the reproducibility error could easily enable comparison of results between different tools.

6 Conclusions

In this work, we performed modeling and regression fitting of IDLS data from a large number of commercial p-type wafers with lightly diffused emitters that contain BO defects. Analysis of the IDLS data set containing $N = 225$ measurements performed after complete deactivation and complete activation of the BO defect revealed that exposure to illumination causes minor but statistically significant changes in lifetime that cannot be attributed to the BO defect alone. This violates a common assumption made during IDLS and TDLS characterization of BO and other CID defects. We also introduced a reduced Chi-square metric that allows for easier interpretation of goodness-of-fit and allows for comparison of goodness-of-fit between samples, analysis methods and potentially, between tools. Based on an analysis of goodness-of-fit and the statistical variability of the capture cross section ratio (k_1) determined from regression fitting for the donor level of BO defect using a number of different methods, it was shown that apart from the BO CID effect, illumination exposure also causes a statistically significant, injection-dependent change in lifetime and a less significant, apparently injection-independent change in lifetime. The former was found to be well modeled by changes in surface passivation while the latter, if present, is hypothesized to be the effect of the acceptor level of the BO defect. While further investigation is required to determine the underlying cause of these effects, ignoring them is expected to introduce additional uncertainties in the determination of k_1 from IDLS and TDLS measurements, in the calculation of normalized defect density and in the determination of defect transition kinetics for BO defects as well as other CID defects.

This study also suggests that the substrate material quality, the presence of diffused emitters, the measurement techniques, and methods used to determine the parameters describing the various components of carrier lifetime can all potentially influence the determination of k_1. A combination of these and other effects explains why a wide range of k_1 values for the BO defect have been previously reported in the literature. Overall, modeling methods that account for changes in surface recombination are expected to be the most accurate for determining k_1. Based on the large data set used in this work, k_1 is determined with a high degree of confidence to be 11.90 ± 0.45 as applied to the fully formed BO defect in low-resistivity, commercial p-type silicon with lightly diffused emitters when modeled using a single-level donor defect. It is predicted that modeling of the acceptor level of the BO defect, performed only in a limited way in this study, is likely to result in a larger and more accurate value of k_1.

Acknowledgements This research has been supported by the Australian Government through the Australian Renewable Energy Agency (ARENA), the Australian Research Council (ARC) and the Australian Centre for Advanced Photovoltaics (ACAP). The views expressed herein are not necessarily the views of the Australian Government, and the Australian Government does not accept responsibility for any information or advice contained herein. The authors would also like to thank the commercial partners of the ARENA 1-060 project, and the UK Institution of Engineering and Technology (IET) for their funding support for this work through the A.F. Harvey Engineering Prize.

References

1. Pingel S, Koshnicharov D, Frank O, Geipel T, Zemen Y, Striner B, Berghold J. Initial degradation of industrial silicon solar cells in

solar panels. In: Proceedings of the 25th European Photovoltaic Solar Energy Conference. Valencia, Spain, 2010, 4027–4032
2. Shockley W, Read W T. Statistics of the recombination of holes and electrons. Physical Review, 1952, 87(5): 835–842
3. Mchedlidze T, Weber J. Direct detection of carrier traps in Si solar cells after light-induced degradation. physica status solidi—Rapid Research Letters, 2015, 9(2): 108–110
4. Schmidt J, Cuevas A. Electronic properties of light-induced recombination centers in boron-doped Czochralski silicon. Journal of Applied Physics, 1999, 86(6): 3175–3179
5. Bothe K, Schmidt J, Hezel R. Effective reduction of the metastable defect concentration in boron-doped Czochralski silicon for solar cells. In: Conference Record of the 29th IEEE Photovoltaic Specialists Conference. New Orleans, USA, 2002, 194–197
6. Rein S, Glunz S W. Electronic properties of the metastable defect in boron-doped Czochralski silicon: unambiguous determination by advanced lifetime spectroscopy. Applied Physics Letters, 2003, 82 (7): 1054–1056
7. Bothe K, Schmidt J. Electronically activated boron-oxygen-related recombination centers in crystallinesilicon. Journal of Applied Physics, 2006, 99(1): 013701
8. Rougieux F E, Forster M, MacDonald D, Cuevas A, Lim B, Schmidt J. Recombination activity and impact of the boron-oxygen-related defect in compensated n-type silicon. IEEE Journal of Photovoltaics, 2011, 1(1): 54–58
9. Voronkov V V, Falster R, Bothe K, Lim B, Schmidt J. Lifetime-degrading boron-oxygen centres in p-type and n-type compensated silicon. Journal of Applied Physics, 2011, 110(6): 063515
10. Wang X, Juhl M, Abbott M, Hameiri Z, Yao Y, Lennon A. Use of QSSPC and QSSPL to monitor recombination processes in p-type silicon solar cells. Energy Procedia, 2014, 55: 169–178
11. Niewelt T, Schön J, Broisch J, Warta W, Schubert M. Electrical characterization of the slow boron oxygen defect component in Czochralski silicon. physica status solidi–Rapid Research Letters, 2015, 9(12): 692–696
12. Niewelt T, Schön J, Broisch J, Rein S, Haunschild J, Warta W, Schubert M C. Experimental proof of the slow light-induced degradation component incompensated n-type silicon. Solid State Phenomena, 2015, 242: 102–108
13. Walter D C, Lim B, Schmidt J. Realistic efficiency potential of next-generation industrial Czochralski-grown silicon solar cells after deactivation of the boron-oxygen-related defect center. Progress in Photovoltaics: Research and Applications, 2016, 24(7): 920–928
14. Hallam B, Abbott M, Nærland T, Wenham S. Fast and slow lifetime degradation in boron-doped Czochralski silicon described by a single defect. physica status solidi—Rapid Research Letters, 2016, 107(7): 509–572
15. Glunz S W, Rein S, Lee J Y, Warta W. Minority carrier lifetime degradation in boron-doped Czochralski silicon. Journal of Applied Physics, 2001, 90(5): 2397–2404
16. Périchaud I. Gettering of impurities in solar silicon. Solar Energy Materials and Solar Cells, 2002, 72(1–4): 315–326
17. Sinton R A, Cuevas A, Stuckings M. Quasi-steady-state photoconductance, a new method for solar cell material and device characterization. In: Conference Record of the 25th IEEE Photovoltaic Specialists Conference. Washington D.C., USA, 1996, 457–460
18. Nagel H, Berge C, Aberle A G. Generalized analysis of quasi-steady-state and quasi-transient measurements of carrier lifetimes in semiconductors. Journal of Applied Physics, 1999, 86(11): 6218
19. Richter A, Werner F, Cuevas A, Schmidt J, Glunz S W. Improved parameterization of auger recombination in silicon. Energy Procedia, 2012, 27: 88–94
20. Cuevas A. The effect of emitter recombination on the effective lifetime of silicon wafers. Solar Energy Materials and Solar Cells, 1999, 57(3): 277–290
21. Schenk A. Finite-temperature full random-phase approximation model of bandgap narrowing for silicon device simulation. Journal of Applied Physics, 1998, 84(7): 3684–3695
22. Couderc R, Amara M, Lemiti M. Reassessment of the intrinsic carrier density temperature dependence in crystalline silicon. Journal of Applied Physics, 2014, 115(9): 093705
23. McIntosh K R, Altermatt P P. A freeware 1D emitter model for silicon solar cells. In: 35th IEEE Photovoltaic Specialists Conference. Honolulu, USA, 2010, 002188–002193
24. Green M A. Intrinsic concentration, effective densities of states, and effective mass in silicon. Journal of Applied Physics, 1990, 67(6): 2944–2954
25. Macdonald D H. Iron detection in crystalline silicon by carrier lifetime measurements for arbitrary injection and doping. Journal of Applied Physics, 2004, 95(3): 1021–1028
26. Thomson A F, McIntosh K R, Macdonald D. Effective lifetime characterisation of a room temperature meta-stable defect in n-type 5 Ω·cm FZ phosphorus-diffused oxide-passivated silicon. In: Proceedings of the 23rd European Photovoltaic Solar Energy Conference. Valencia, Spain, 2008, 517–521
27. Andrae R, Schulze-Hartung T, Melchior P. Dos and don'ts of reduced chi-squared. 2016–07, http://122.physics.ucdavis.edu/sites/default/files/files/Error%20Analysis/chi-sq-1012.3754.pdf
28. McIntosh K R, Sinton R A. Uncertainty in photoconductance lifetime measurements that use an inductive-coil detector. In: Proceedings of 23rd European Photovoltaic Solar Energy Conference. Valencia, Spain, 2008, 77–82
29. Blum A L, Swirhun J S, Sinton R A, Yan F, Herasimenka S, Roth T, Lauer K, Haunschild J, Lim B, Bothe K, Hameiri Z, Seipel B, Xiong R, Dhamrin M, Murphy J D. Interlaboratory study of eddy-current measurement of excess-carrier recombination lifetime. IEEE Journal of Photovoltaics, 2014, 4(1): 525–531
30. Haynes J R, Hornbeck J A. Temporary traps in silicon and germanium. Physical Review, 1953, 90(1): 152–153
31. Cousins P J, Neuhaus D H, Cotter J E. Experimental verification of the effect of depletion-region modulation on photoconductance lifetime measurements. Journal of Applied Physics, 2004, 95(4): 1854–1858
32. Seiffe J, Gautero L, Hofmann M, Rentsch J, Preu R, Weber S, Eichel R A. Surface passivation of crystalline silicon by plasma-enhanced chemical vapor deposition double layers of silicon-rich silicon oxynitride and silicon nitride. Journal of Applied Physics, 2011, 109 (3): 034105
33. Liao B, Stangl R, Mueller T, Lin F, Bhatia C S, Hoex B. The effect of light soaking on crystalline silicon surface passivation by atomic layer deposited Al_2O_3. Journal of Applied Physics, 2013, 113

(2): 024509

34. Sperber D, Herguth A, Hahn G. On the stability of dielectric passivation subjected to illumination and temperature treatments on the stability of dielectric passivation. In: Proceedings of the 26th European Photovoltaic Solar Energy Conference. Munich, Germany, 2016
35. Seiffe J, Hofmann M, Rentsch J, Preu R. Charge carrier trapping at passivated silicon surfaces. Journal of Applied Physics, 2011, 109 (6): 064505
36. Murphy J D, Bothe K, Krain R, Voronkov V V, Falster R J. Parameterisation of injection-dependent lifetime measurements in semiconductorsin terms of Shockley-Read-Hall statistics: an application to oxide precipitates in silicon. Journal of Applied Physics, 2012, 111(11): 113709
37. Niewelt T, Schön J, Broisch J, Mägdefessel S, Warta W, Schubert M. A unified parameterization of the formation of boron oxygen defects and their electrical activity. Energy Procedia, 2016, 92: 170–179
38. Niewelt T, Mägdefessel S, Schubert M. Fast in-situ photoluminescence analysis for a recombination parameterization of the fast BO defect component in silicon. Journal of Applied Physics, 2016, 120 (8): 085705
39. Bothe K, Hezel R, Schmidt J. Understanding and reducing the boron-oxygen-related performance degradation in Czochralski silicon solar cells. Solid State Phenomena, 2004, 95: 223–228
40. Hamer P, Nampalli N, Hameiri Z, Kim M, Chen D, Gorman N, Hallamb B, Abbottb M, Wenhamb S. Boron-oxygen defect formation rates and activity at elevated temperatures. Energy Procedia, 2016, 92: 791–800
41. Nakayashiki K, Hofstetter J, Morishige A E, Li T A, Needleman D B, Jensen M A, Buonassisi T. Engineering solutions and root-cause analysis for light-induced degradation in p-type multicrystalline silicon PERC modules. IEEE Journal of Photovoltaics, 2016, 6(4): 860–868